Supplement to:

Intracellular single molecule microscopy reveals time and mRNA dependent microRNA assembly

Sethuramasundaram Pitchiaya[1], John R. Androsavich[1,2] & Nils G. Walter[1+]

[1]Department of Chemistry, Single Molecule Analysis Group, [2]Program in Chemical Biology, University of Michigan, Ann Arbor, MI 48109–1055, USA.

[+]Corresponding author: E-mail: nwalter@umich.edu.

CONTENTS:

SUPPLEMENTARY FIGURE LEGENDS

Supplementary Figure S1 | Precision and signal intensity of live cell imaging, and cxcr4 control experiments. (**A**) Precision of single particle localization. Histogram depicting the displacement of formaldehyde-fixed let-7-a1-Cy5 particles about their origin (n = 100 randomly selected particles). The location of each particle was tracked over time until it photobleached. The histogram was fit with a Gaussian function, which resulted in a mean of ~30 nm and a standard deviation of ~50 nm. Large jumps (>100 nm) were observed only when there were large fluctuations of intensity. Localization precision of immobilized beads (inset) was ~4 nm, largely owing to their higher signal-to-noise ratio (n = 100 randomly selected particles). (**B**) Signal intensities of particles undergoing diffusion in living cells. Intensity time trajectories of let-7-a1-Cy3 (green) and let-7-a1-Cy5 (red) particles are shown. Trajectories of both mobile and static particles are shown, as indicated in each trajectory. A significant proportion of particles had a relatively constant intensity during diffusion before disappearing. We infrequently observed large fluctuations in intensity as a particle was diffusing, possibly due to diffusion in the axial dimension (z-axis). We also occasionally observed stepwise changes in intensity of static particles, possibly due to photobleaching (see, for example, second trajectory from the top on the left side). (**C-E**) Intracellular diffusion of cxcr4 miRNA, with (**C**) DIC image and (**D**) the corresponding pseudocolored image of a cell microinjected with cxcr4-Cy3 and imaged 4 h after injection. Scale bar, 10 μm. (**E**) Distribution of diffusion coefficients calculated from individual MSD plots of cxcr4-Cy3. We observed two major Gaussian distributions, with different fractional abundance but average diffusion coefficients similar to those obtained with let-7-a1-Cy3.

Supplementary Figure S2 | Tracking the diffusion of individual PBs in live HeLa cells. (**A**) Representative PBs demonstrating confined (i) and Brownian motion (ii). (**B**) MSD over time of the particles in A. Diffusion coefficients calculated from the plot were D(i) = 0.0007 $\mu m^2/s$ and D(ii) = 0.026 $\mu m^2/s$. (**C**) Distribution of diffusion coefficients of Dcp1a foci in live HeLa cells (n = 15 cells, 192 particles). The distribution bears strong resemblance to the slowly diffusing miRNA population (**Fig 2F, G**).

Supplementary Figure S3 | Live cell images after incubation for varying amounts of time after microinjection. (**A**) Representative images of cells incubated for 5 min to 32 h after microinjection, as indicated. Dashed and dotted lines indicate nuclear and cellular boundaries, respectively. Scale bar, 10 μm. (**B**) Analysis of background intensity and average number of nine-consecutive-frame localizations. The relative average background intensity (black, solid), which reflects blurred, rapidly diffusing particles, was calculated for each time point and the resultant curve fitted with a single-exponential decay function, yielding a rate constant of 0.82 ± 0.18 h^{-1}. The highest background intensity was found at the earliest time point and continually decreased, consistent with the notion that miRNAs increasingly assemble into large, slowly diffusing, and thus less blurred (at a time resolution of 100 ms) RNPs over this time frame. To quantify assembly further, we determined the average number of particles at each time point that were visible for at least nine consecutive video frames (grey, dashed), a lower bound we used for our diffusion coefficient calculation. The data fit well with a double-exponential function with a rapid-rise phase characterized by a rate constant of 1.18 ± 0.62 h^{-1}, indicating assembly of miRNAs into larger RNPs (especially over the first 2 h of observation), and a slower decrease phase with a rate constant of 0.34 ± 0.13 h^{-1}, indicating an increase in RNP mobility over a longer time frame (2 h – 32 h). These kinetically distinct processes and their rate constants are

similar to those obtained in our fixed-cell photobleaching analysis ($1.18 \pm 0.18\ h^{-1}$, $0.14 \pm 0.08\ h^{-1}$ and **Fig. 4E**, black lines), further supporting our model that a relatively rapid initial assembly of miRNAs into large RNPs is followed by slow disassembly at later times. Error bars, standard error of the mean (n = 4, 4, 4, 6, 4 cells for 1, 2, 4, 8, 32 h samples respectively).

Supplementary Figure S4 | Relative deviation (RD) analysis of diffusion coefficients over time. Histograms depict the distribution of RD values (**Supplementary Methods**) at different times after let-7-a1-Cy5 microinjection (2 h, 4 h and 8 h, as indicated). RD values were calculated using MSD values corresponding to the sixth localization point and diffusion coefficients extracted from the first three points of the MSD time course. Although the distributions differ slightly, there is no significant increase in the fraction of higher RD values which, if present, would predict an increase in the fraction of particles undergoing directed motion (n = 4 cells for each, **Supplementary Table 1**).

Supplementary Figure S5 | Stepwise photobleaching in fixed cells. (**A**) Additional examples of stepwise photobleaching traces. (**B-D**) Control experiments. (**B**) Pseudo-colored, background subtracted image of cell microinjected with double-stranded DNA probe MS2 labeled with ~3.45 Cy5s per molecule. Outlines of the cell (dotted) and its nucleus (dashed) are also shown. Scale bar, 10 μm. (**C**) Types of photobleaching observed from experiment in **B**. (**D**) Distribution of photobleaching steps for MS2-Cy5 injections (n = 3 cells, 702 particles). Error bars, standard deviation. (**E**) Comparison of fluorescence intensities of Cy5-labeled miRNA-containing particles between living (grey) and fixed cells (black), imaged 2 h after microinjection. Only diffusing particles visible in live cells for 9 frames or longer were included in the analysis. The intensity observed in the first frame of each video (100 ms exposure time) was used to create this histogram (n = 4 cells each).

Supplementary Figure S6 | Representative images and resulting stepwise photobleaching distributions from fixed cells incubated for various amounts of time after microinjection. Shown are (from left to right) DIC, pseudo-colored, pseudo-colored/background-subtracted images and photobleaching step distributions of cells injected with let-7-a1-Cy5 and fluorescein dextran. Images and distributions were taken from cells fixed (**A**) 20 min, (**B**) 1 h, (**C**) 2 h, (**D**) 4 h, (**E**) 8 h and (**F**) 32 h after microinjection ($n_{B\text{-}F}$ = 5, 4, 3, 4, 8 cells and 1,125, 1,509, 940, 1,168, 688 particles respectively). Error bars, standard deviation. Scale bar, 10 μm. The background was very high in cells incubated for 20 min after microinjection, thus it was practically impossible to locate single molecules.

Supplementary Figure S7 | miRNAs assembly is mRNA dependent. (**A**) Schematic of 5' capped (black dot) and 3' poly-A tailed mRNAs. RL mRNA (top) is a negative control that contains only the coding sequence of renilla luciferase. RL-cxcr4-6x mRNA (bottom) is the target that contains the same renilla luciferase coding sequence plus six cxcr4 binding sites as indicated in the magnified view. (**B**) Distribution of monomers and multimers in cells that were microinjected with cxcr4 miRNA and no mRNA, with cxcr4 miRNA and RL mRNA, or with cxcr4 miRNA and RL-cxcr4-6x mRNA. The inset shows the distribution further divided into one, two and three or more photobleaching steps in these samples. Even though a significant increase in the number of multimers was observed upon co-microinjection of cxcr4 miRNA with its target RL-cxcr4-6x mRNA, a specific enrichment of particles bearing six miRNAs was not seen, suggesting sub-stoichiometric binding of miRNAs to target mRNA binding sites. Error bars, standard deviation (n = 4 cells for each of the samples). (**C**) Distribution of monomers and multimers of mutant let-7-a1 miRNA non-colocalized (independent) or colocalized with MS2-GFP tagged target mRNAs (see **Fig 3B, C**). The coordinates of stepwise-photobleached particles

in the mut-let-7-Cy5 channel were mapped to the mut-mRNA-EGFP channel to assess the extent of colocalization. N = 2 cells containing a total of 60 independent and 16 colocalized let-7-a1 particles. Data points within each group are explicitly shown (grey circles, monomers; black squares, multimers) in addition to their mean values (grey dotted line, monomers; black dotted line, multimers). The statistical variation within each group was minimal between replicates.

Supplementary Figure S1

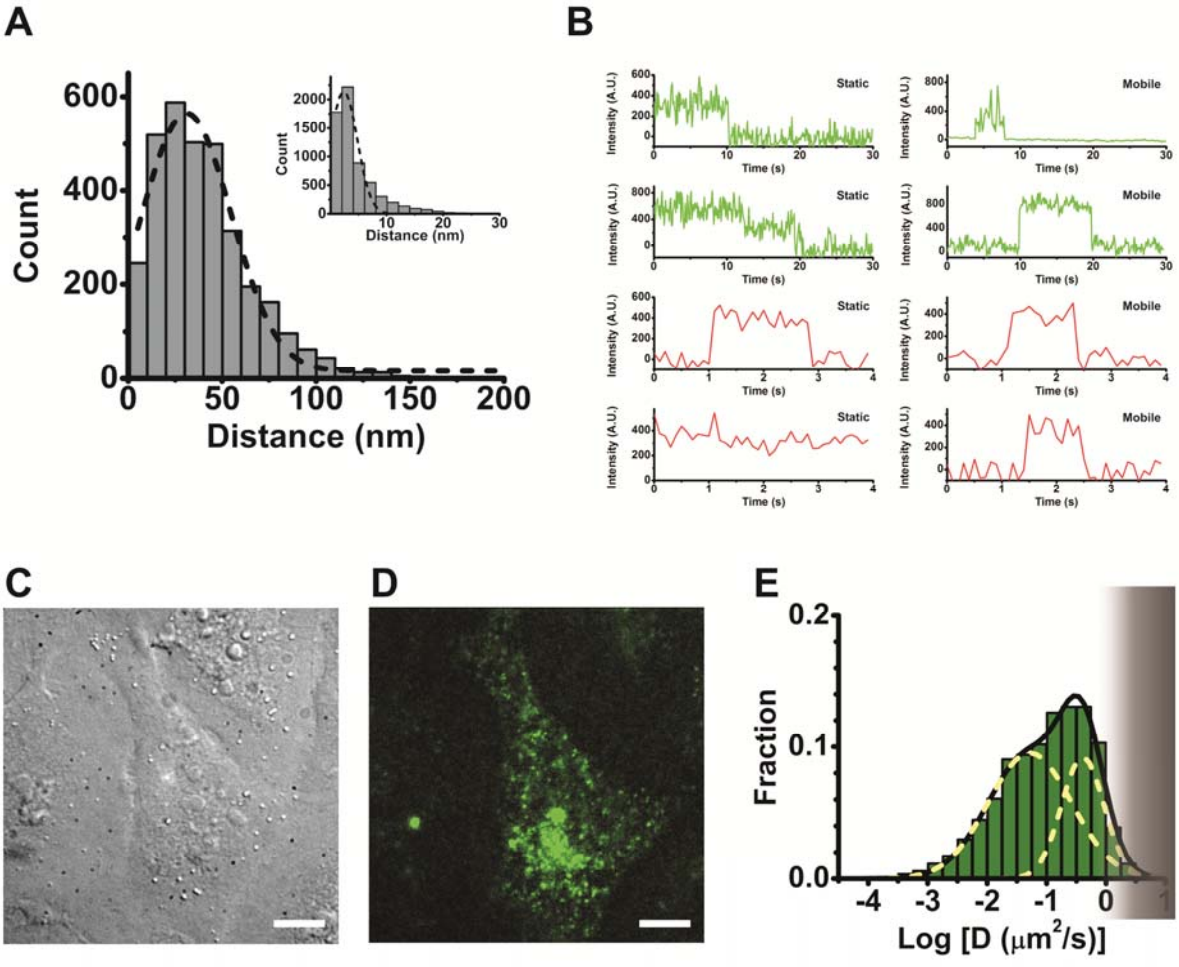

Supplementary Figure S2

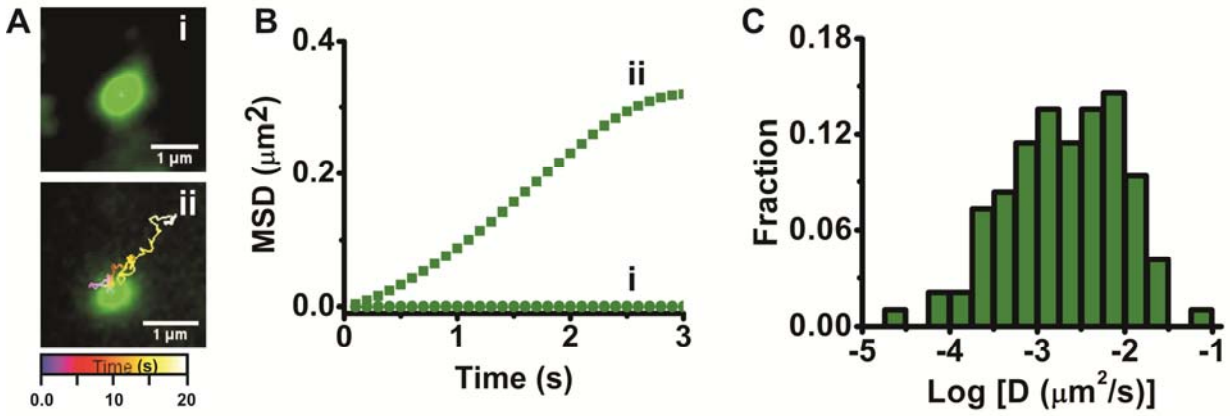

Supplementary Figure S3

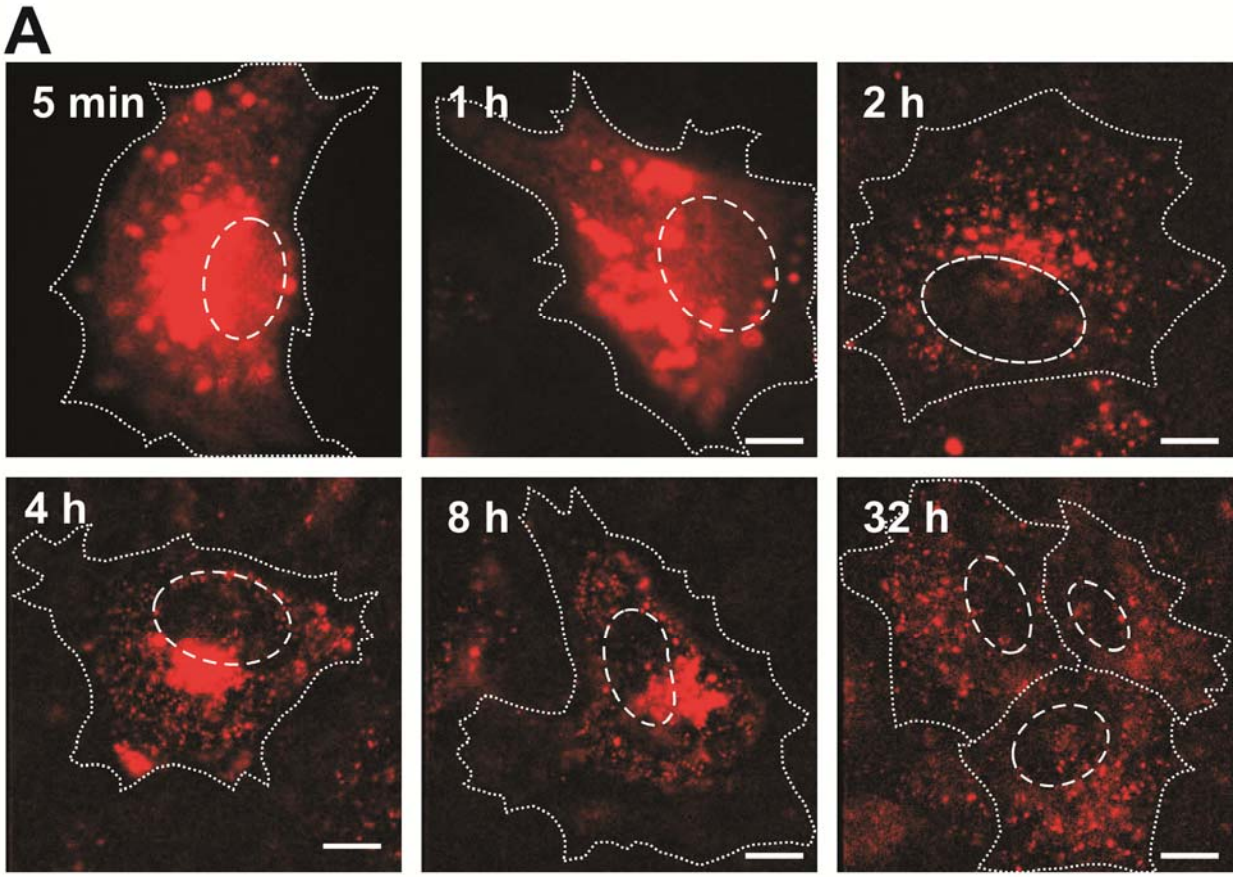

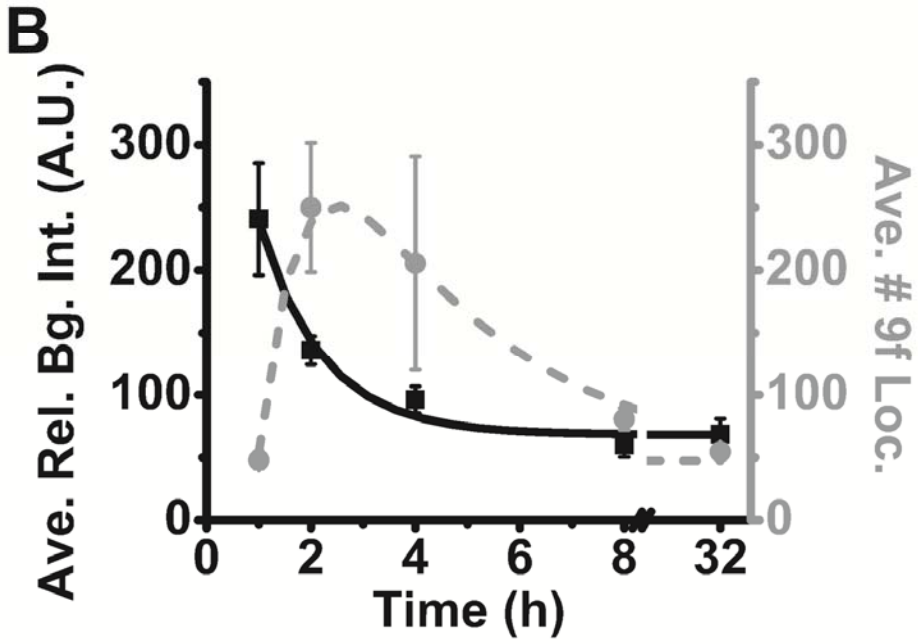

Supplementary Figure S4

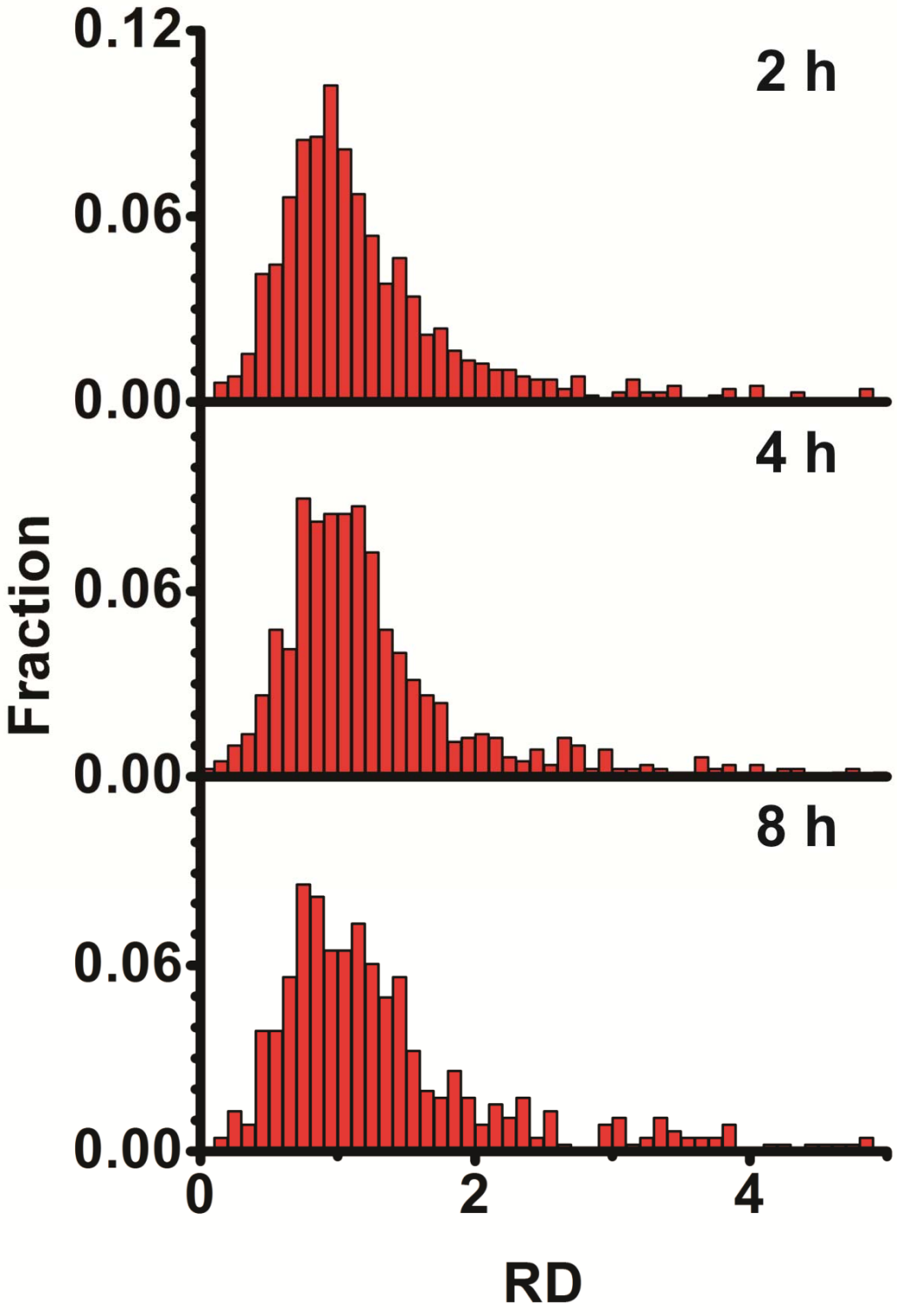

Supplementary Figure S5

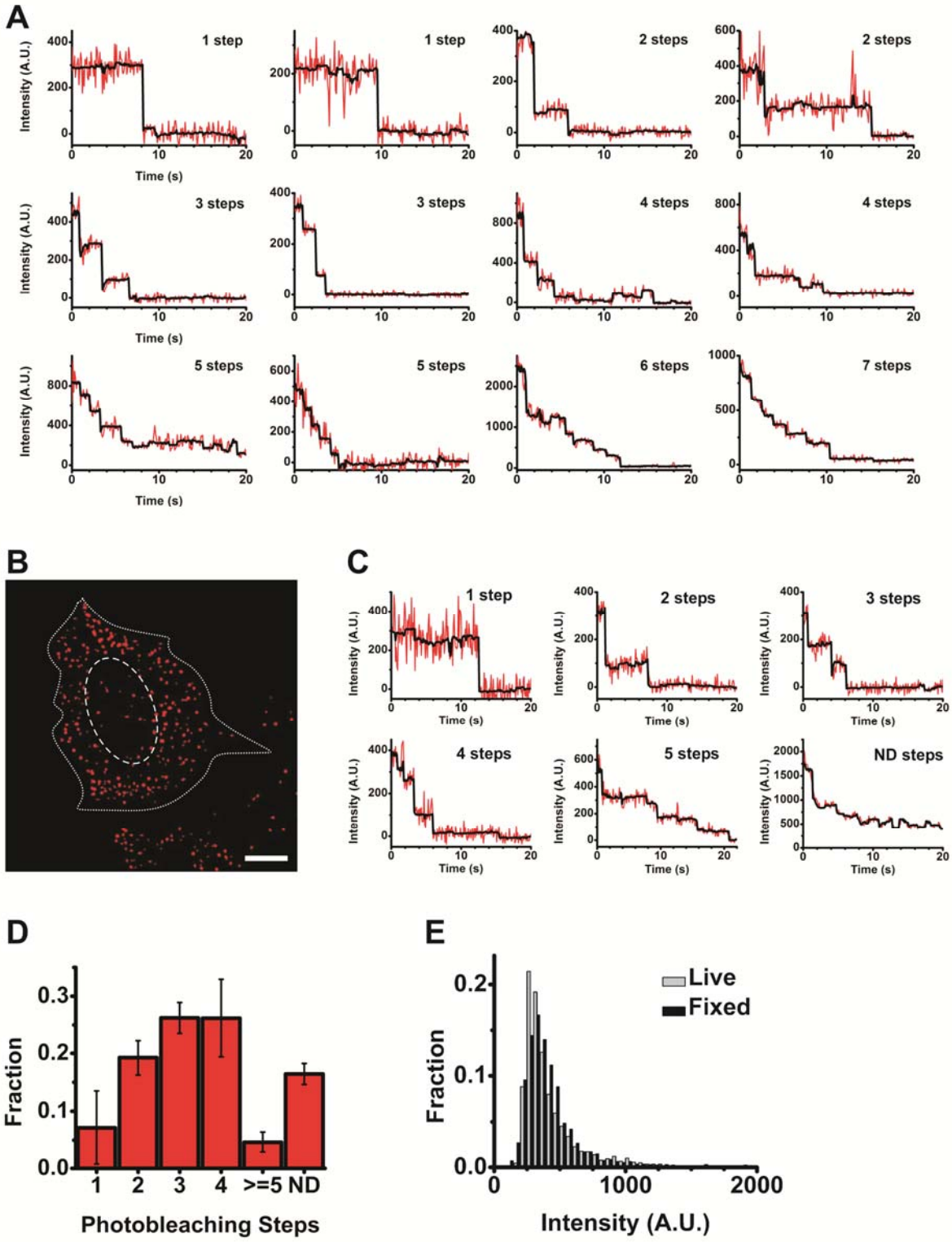

Supplementary Figure S6

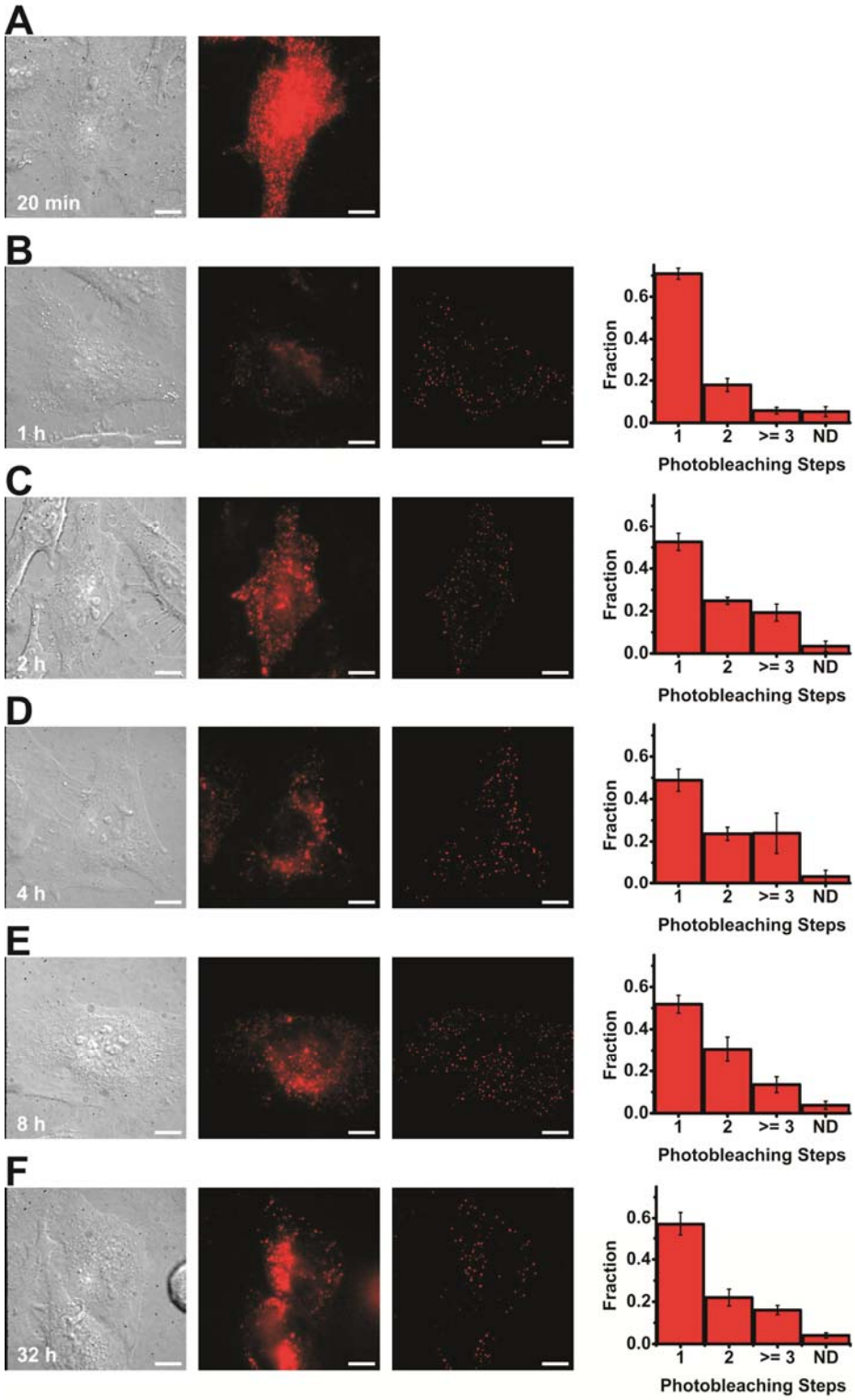

Supplementary Figure S7

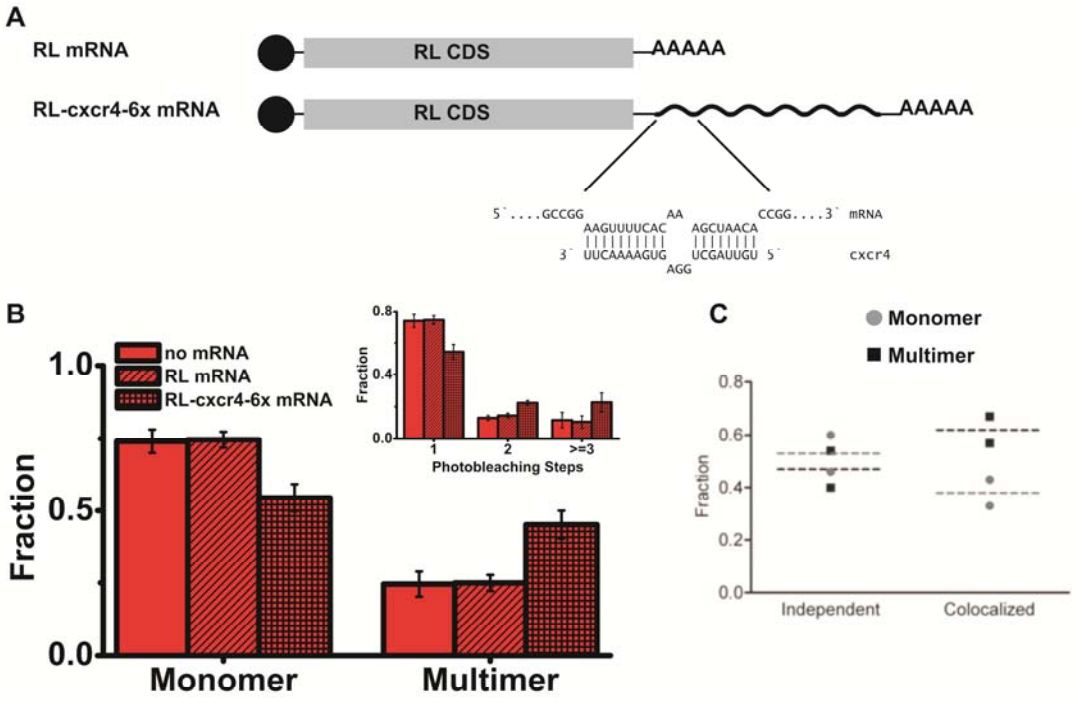

SUPPLEMENTARY VIDEO LEGENDS

Supplementary Video 1 | Videos of Cy3 and Cy5 labeled miRNAs diffusing in living HeLa cells. (**A**) Pseudo-colored, 300-frame (30 s) video of two cells injected with let-7-a1-Cy3 in the cytosol (left) and nucleus (right), respectively, imaged 4 h after microinjection. (**B**) Pseudo-colored 50-frame (5 s) video of a cell microinjected in the cytoplasm with let-7-a1-Cy5 (and fluorescein dextran) imaged 2 h after injection. The speed of both videos was increased to 30 frames/s (acquisition rate was 10 frames/s) to aid in viewing diffusing particles.

Supplementary Video 2 | Different types of diffusive motions exhibited by miRNAs. (**A**) An immobile particle. (**B**) Particle undergoing Brownian motion. (**C**) Particle exhibiting biased motion. (**D**) Particle exhibiting corralled motion. All videos shown here are from cells microinjected with let-7-a1-Cy3, imaged 4 h after microinjection. Time scales represent 4 s, 10.7 s, 9 s and 16 s, respectively. Center of particle is labeled with a grey circle to aid visualization.

Supplementary Video 3 | Live cell imaging control experiments. (**A**) Video of cells injected with phosphate buffered saline (PBS), and imaged with 532 nm excitation. (**B**) Video of cells microinjected with fluorescein dextran and imaged with 640 nm excitation. We see ~10 to 20 false-positive particles, but cells injected with the miRNA had almost ten-fold more spots. The number of false-positive particles was higher with 532 nm excitation as compared to 640 nm excitation, as expected from the higher autofluorescence of cells at shorter wavelengths.

Supplementary Video 4 | Pseudo-colored video showing photobleaching of let-7-a1-Cy5 miRNAs in fixed cells, imaged 2 h after microinjection. The speed of the video was increased to 30 frames/s (acquisition rate was 10 frames/s).

SUPPLEMENTARY TABLE

Supplementary Table 1 | Number of cells and particles used in both live and fixed cell analysis.

Live cell analysis			
Experiment	**No. cells (no. particles*)**	**Initial no. particles*/frame**	**No. frames/video**
Cy3 labeled miRNAs			
Let-7-a1, 4 h post-injection	4 (2115)	95	300
Cxcr4, 4 h post-injection	3 (1038)	115	300
Let-7-a1-Cy5			
1 h post-injection	4 (240)	45	50
2 h post-injection	4 (1000)	251	50
4 h post-injection	4 (822)	295	50
8 h post-injection	6 (484)	90	50
32 h post-injection	4 (109)	21	50
Fixed cell analysis			
Experiment	**# cells (# particles)**	**Average # particles/cell**	**# frames/video**
	Let-7-a1, *cxcr4, cxcr4+ RL-cxcr4-6x mRNA*		
1 h post-injection	5 (1125), *5 (1414), 4 (1295)*	225 ± 121, *236 ± 71, 324 ± 49*	300, *500, 400*
2 h post-injection	4 (1509), *5 (1500), 4 (1012)*	377 ± 72, *300 ± 118, 253 ± 43*	300, *500, 400*
RL mRNA	*4 (1150)*	*288 ± 102*	*300*
4 h post-injection	3 (940), *5 (1210), 4 (1263)*	313 ± 158, *242 ± 99, 316 ± 61*	300, *500, 400*
8 h post-injection	4 (1168), 7 *(1825), 6 (1525)*	292 ± 166, *261 ± 187, 254 ± 131*	300, *500, 400*
32 h post-injection	8 (688), *9 (1294), 8 (1232)*	86 ± 34, *144 ± 49, 154 ± 65*	300, *500, 400*
MS2-Cy5 DNA	3 (702)	234 ± 125	300

*particles visible for greater than 9 frames

SUPPLEMENTARY METHODS

Plasmids, DNA and RNA olignucleotides. Luciferase reporter plasmids pmG-mH3U (wt) and pmG-mH3UM (mut) were engineered by inserting the wild-type and mutant mouse HMGA2 3' UTR sequences, respectively, downstream of the firefly luciferase ORF in the pmirGLO dual-luciferase expression vector (Promega). The wild-type and mutant 3' UTRs were PCR amplified from plasmid templates received as a gift from David Bartel (Whitehead Institute, MIT) [1] using primers containing at their 5' ends XhoI and NotI or XhoI and XbaI restriction sequences, respectively. Following restriction digestion, the amplicon insert was ligated to complementary ends in the pmirGLO vector. Fluorescence reporter plasmid pEF6-mCherry-mH3Um was constructed by first subcloning the mCherry ORF from the pRSET-mCherry vector, a gift from Roger Tsien (UCSD), into the multiple cloning site of the pEF6-myc-His-B (Invitrogen) vector using BamHI and EcoRI restriction sites. Then, using PCR cloning, the mutant HMGA2 3' UTR was inserted downstream of the mCherry ORF between XhoI and NotI sites. pEGFP-C1 was purchased from Clontech. pMCP-EGFP, a plasmid bearing the ORF of the MS2 coat protein fused to EGFP and an SV-40 nuclear localization signal (NLS), and pSL-MS2_24x, a plasmid bearing 24 copies of the MS2 stem loops [2], were received as gifts from Robert Singer (Albert Einstein College of Medicine). A Luciferase reporter plasmid bearing the MS2 stem loops was created in two steps. First, the ORF of IF2, PCR amplified using a forward primer bearing SbfI and EcoRI restriction enzyme sites and a reverse primer bearing a NotI restriction enzyme site, was cloned into the corresponding SbfI and NotI sites in plasmid pmG-mH3UM. 24 copies of the MS2 stem loop (from pSL-MS2_24x) were then cloned into the EcoRI-NotI restriction enzyme sites of the resultant plasmid, pmG-mH3UM-IF2, to generate pmG-mH3UM-MS2. We had to resort to this two-step procedure because linearized plasmids containing the MS2 stem loops

often recombined with the genome of the bacterial competent cells we were using, thus resulting in clones bearing smaller plasmids. Clones containing the MS2 stem loops were created in SURE2 bacterial cells (Stratagene) to minimize recombination of the MS2 repeats with the bacterial genome. Plasmid pEGFP-hDcp1a was created by removing the mRFP1 ORF from pmRFP1-hDcp1a (gift from Nancy Kedersha, Brigham Women‘s hospital) using AgeI and XhoI restriction enzyme digestion and replacing it with the similarly digested ORF of EGFP, which was PCR amplified from pEGFP-C1 (Clontech) using DNA primers bearing AgeI and XhoI restriction enzyme sites. Plasmid pRL-TK-cxcr4-6x [3], containing the renilla luciferase coding sequence and an artificial 3’ UTR with six binding sites for an artificial cxcr4 miRNA downstream of the T7 promoter, was purchased from Addgene.

Negative control siRNA used in transfection experiments was purchased from Ambion. SiLuc2 siRNA, a positive control siRNA, was designed towards the coding sequence of the firefly luciferase gene (*luc2*) and purchased from Dharmacon as a duplex. All other RNA oligonucleotides were purchased from the Keck Biotechnology Resource Laboratory at the Yale University School of Medicine with a 5’ phosphate (P) and, in the case of amine modified RNA, a 3’ amino group on a C7 carbon linker. RNA was purified as described [4] and the 3’ amine groups were labeled with Cy3 or Cy5 succinimidyl ester as described [4, 5]. RNA sequences were as follows:

let-7-a1 guide: P-UGAGGUAGUAGGUUGUAUAGUU

let-7-a1-passenger: P-CUAUACAAUCUACUGUCUUUCC

let-7-a1 mut guide: P-UGCGUUAGUAGGUUGUAUAGUU

let-7-a1 mut passenger: P-CUAUACAAUCUACUGUCGUUCC

cxcr4 guide: P-UGUUAGCUGGAGUGAAAACUU

cxcr4 passenger: P-GUUUUCACAAAGCUAACACA

siLuc2 guide: GAAGUGCUCGUCCUCGUCCUU

siLuc2 passenger: GGACGAGGACGAGCACUUCUU

Guide and passenger strands were heat-annealed in a 1:1 ratio, resulting in duplex miRNAs, and frozen for further use. DNA oligonucleotide MS2 with four internal amine modifications was purchased from the Keck Biotechnology Resource Laboratory at the Yale University School of Medicine, purified and labeled as described above. A DNA oligonucleotide completely complementary to MS2 (C-MS2) with a 5' phosphate (P) was purchased from Invitrogen. The labeled and complementary strands were annealed in a 1:1 ratio and frozen for further use. DNA sequences were as follows:

MS2: AXGTCGACCTGCAGACAXGGGTGATCCTCAXGTTTTCTAGGCAATXA

(X represents an amine modified deoxy-uridine)

C-MS2: P-TAATTGCCTAGAAAACATGAGGATCACCCATGTCTGCAGGTCGACAT

mRNA synthesis. pRL-TK-cxcr4-6x was linearized either with XhoI or NotI restriction enzyme and purified by phenol-chlorofom extraction followed by ethanol precipitation. *In vitro* transcriptions were performed with 1 μg linearized plasmids using the MegaScript T7 kit (Ambion) according to manufacturer's protocol. Transcription reactions were then DNase treated (turbo DNase, Ambion) and the respective RNAs, RL (XhoI digest) and RL-cxcr4-6x (NotI digest), purified by LiCl precipitation. The RNAs were size selected from upon 5% (w/v) urea poly-acrylamide gel electrophoresis, 5'capped with m^7G using the ScriptCap capping kit and polyadenylated using the polyA tailing kit (Epicentre). Capped and tailed RNAs were purified by

gel filtration (Roche© RNA columns). The length of the polyA tails was estimated based on electrophoretic mobility on a 1.2% formaldehyde agarose gel.

Cell culture and media. HeLa cells (CCL-2, ATCC) were cultured in DMEM (GIBCO, Invitrogen) supplemented with 10% (v/v) fetal bovine serum (FBS) and non-essential amino acids (NEAA) at 37 ^{o}C. 1 - 1.25 x 10^5 cells were seeded onto delta-T dishes (Bioptechs) one day before microinjection, such that they were ~80% confluent at the time of microinjection. Regular medium was replaced with phenol red-free medium 4 h prior to microinjection and subsequently with a minimal medium (HBS), without serum and vitamins, but containing 20 mM HEPES-KOH pH 7.4, 135 mM NaCl, 5 mM KCl, 1 mM $MgCl_2$, 1.8 mM $CaCl_2$ and 5.6 mM glucose, immediately before microinjection. After microinjection, cells were incubated in phenol red-free DMEM containing 2% (v/v) FBS and 1x NEAA and in the presence of a 5% CO_2 atmosphere for the indicated amounts of time prior to imaging. For long incubations (4 h and greater), the medium was replaced every 4 h with fresh growth medium containing 2% (v/v) FBS. We found that cellular autofluorescence was a function of serum concentration; higher serum concentrations resulted in higher background and medium with no serum exhibited the least background. We used 2% (v/v) FBS to prevent conditions of serum starvation and simultaneously minimize cellular autofluorescence.

Microinjection. Microinjections were performed using a Femtojet pump (Eppendorf) and a microscope mounted Injectman NI2 micromanipulator (Eppendorf). Solutions to be microinjected were centrifuged at 16,000 x g for 15 min at 4^{o}C just prior to microinjection. For a

majority of the tracking and fixed cell experiments, the micropipette (Femtotips, Eppendorf) was loaded with 1.5 μM fluorophore labeled miRNA and 0.05% 10 kDa Fluorescein dextran (Invitrogen) in PBS. Fluorescein, which is spectrally distinct from Cy5, served as a marker to locate microinjected cells, mainly because Cy5 photobleached relatively quickly (within ~1.5 s). The focal plane to be imaged was adjusted during 488 nm (fluorescein) excitation and then quickly switched to 640 nm (Cy5) excitation for image acquisition. For (negative) control experiments (**Supplementary Video 3**), the miRNA was omitted and either 0.05% Fluorescein dextran (Invitrogen) in PBS or plain PBS were used. Microinjection of fluorescein dextran only resulted in very low background and false-positive particles (**Supplementary Video 3B**). In some experiments, the fluorescein dextran was omitted and 2 μM Cy3 labeled miRNA in PBS was used. Although Cy3 labeled particles were visible for a longer time than those of Cy5, the majority of experiments were performed with Cy5 labeled miRNAs in conjunction with fluorescein dextran for two reasons: (i) cellular autofluorescence was higher upon 532 nm (Cy3) excitation as compared to 640 nm excitation; and (ii) it was easier to choose microinjected cells and check for microinjector clogging without photobleaching the dye conjugated to the miRNA. Co-microinjecting let-7-a1-Cy3 along with either fluorescein dextran or Alexa-647 dextran resulted in high background fluorescence and strong Cy3 fluorescence quenching, respectively, when illuminated with at 532 nm. The former background is largely contributed by the spectral overlap between fluorescein and Cy3. For MS2 DNA microinjections, 0.5 μM duplex DNA mixed with 0.05% (w/v) of 10 kDa fluorescein dextran in PBS was microinjected. For co-microinjections of miRNA with mRNA, 1.5 μM cxcr4 miRNA and 0.25 μM mRNAs (RL or RL-cxcr4-6x) were mixed with 0.05% (w/v) of 10 kDa fluorescein dextran in PBS. All of the above microinjections were performed at 100 hPa microinjection pressure for 0.5 s with 20 hPa

compensation pressure. Using these conditions, microinjection volume was estimated to be ~0.02 pL or ~0.5% - 5% of the total cell volume, which translates to ~18,000 molecules of miRNA (at 1.5 μM working concentration). For plasmid microinjections, compensation pressure was increased to 40 hPa and plasmids were co-microinjected along with the appropriate amounts of miRNA at a working concentration of 0.1 μg/μl in PBS (see **Repression Assays** for further details).

Fluorescence microscopy. Imaging was performed using a cell-TIRF system based on an Olympus IX81 microscope equipped with a 60x 1.45 NA oil-immersion objective (Olympus), nanometer-precision motorized stage (ASI Imaging), focal drift control module (zero drift control, Olympus), 1x – 4x magnification changer (Olympus) and an EM-CCD camera (Evolve, Photometrics). Solid state lasers with wavelengths of 488 nm (25 mW), 532 nm (100 mW) and 640 nm (100 mW), were directed through an acousto-optical tunable filter, split into different fiber-optic cables and then coupled to the cell-TIRF module. All laser lines had 10 nm bandwidth clean-up filters to ensure monochromatic illumination. Net powers of ~1.2 mW, 7 mW and 8 mW were achieved at the objective for the 488 nm, 532 nm and 640 nm laser lines, respectively. Laser beams were focused on the back-focal plane of the objective and made to travel parallel to the optic axis such that changing the distance from the optic axis controlled incident angle at the dish-media interface. Highly inclined laminar optical sheet (HILO) microscopy [6] was used to achieve deeper penetration into cells without compromising on signal-to-noise ratio. A dual band filter cube consisting of a z491/639rpc dichroic filter (Chroma) and z491/639m emission filter (Chroma) was used to detect GFP and Cy5 emission. Cy3 emission was detected using a Q570LP dichroic filter (Chroma) and HQ610/75m emission filter (Chroma). All videos were

recorded at 100 ms camera exposure time using 120x magnification (60x objective and 2x additional magnification using the magnification changer) unless otherwise mentioned. Cells were maintained at 37 ^{o}C on the microscope stage while imaging using the DeltaT open dish system (Bioptechs) and a heated lid (Bioptechs). 5% CO_2 was supplemented to cells using the side port of the heated lid.

Live cell imaging data analysis. The dish was washed several times with HBS immediately after microinjection. Cells were imaged in HBS consisting of 0.3 U/mL Oxyfluor (Oxyrase), 20 mM sodium succinate, 2 mg/mL ascorbic acid and 200 μM trolox (HBS-OSS). Oxyfluor and its substrate succinate act as an oxygen scavenging system, whereas ascorbic acid and trolox served as strong triplet state quenchers, effectively increasing the lifetime of the fluorophores inside the cells.

Single particles were tracked using the tracking module of Imaris (Bitplane). Only particles that lasted for more than 9 frames, in which case the error in the calculated diffusion coefficient will be ~50% [7], were used for further analysis. All tracks were visually inspected to ensure that they arose from well-isolated particles. In-house MATLAB routines were then used to calculate the mean squared displacement (MSD) and diffusion coefficients. Brownian diffusion coefficients were calculated by fitting the mean squared displacement for the first three time intervals to the equation [8]:

$$\langle \boldsymbol{r^2} \rangle = \boldsymbol{4D\Delta t + offset}$$

An offset was used to account for the error in localization at t = 0. Localization precision was measured by tracking the variation in position of fixed miRNA particles (**Supplementary Fig.**

S1A). Relative deviation analysis [9] was performed on individual trajectories, based on the equation:

$$\boldsymbol{RD = \frac{MSD\ (n)}{4Dn\Delta t}}$$

where D is the instantaneous diffusion coefficient and n is a data point at a later time lag, not included in the original calculation of D. An RD value of 1 corresponds to pure Brownian motion. If the MSD time course were to deviate from linearity, such as those in anomalous, directed and corralled motions, RD values will deviate from 1. Thus, by comparing the distribution of RD values between multiple sample sets, we can gauge if a change in mobility of particles is due to the preponderance of one type of diffusive pattern over another.

The analytical forms of MSD time courses for different forms of motion:

$$\boldsymbol{\langle r^2 \rangle = 4D\Delta t + offset} \qquad \text{(Brownian motion)}$$

$$\boldsymbol{\langle r^2 \rangle = \langle r_c^2 \rangle \left[1 - A_1 e^{(-4A_2 D\Delta t / \langle r_c^2 \rangle}\right] + offset} \qquad \text{(Corralled motion)}$$

$$\boldsymbol{\langle r^2 \rangle = 4D\Delta t + (Vt)^2 + offset} \qquad \text{(Biased / directed motion with diffusion)}$$

were used to derive diffusion coefficients from data points in Fig. 1e respectively.

Calculation of background intensity was done using ImageJ software (NIH). Briefly, a binary mask, using the background subtracted-thresholded image created by our intensity analysis software (see **Fixed cell imaging and data analysis**), was used to subtract all miRNA particles from an image and the total intensity from the resultant image was used to calculate the average background intensity. Intensity of regions outside the cell was used as the baseline to calculate the relative average background intensity.

The 1 h and 32 h datasets were background subtracted, thresholded and deconvolved to accurately localize single particles. These images were subsequently also used in **Supplementary Fig. S4** to calculate the average number of particles visible for at least nine consecutive frames.

Fixed cell imaging and data analysis. Cells were first washed five times with PBS, fixed using 4% (w/v) paraformaldehyde in PBS for 20 min, washed five times with PBS after fixing and imaged in PBS consisting of the same OSS-antioxidant mix as mentioned above (PBS-OSS).

Intensity analysis to determine number of photobleaching steps was performed using a custom written LabView (National Instruments) code [10]. A Chung-Kennedy non-linear filter [11] was used to effectively average out the noise within intensity traces, yet preserving fast and sudden transitions, which aided in better visualization of photobleaching steps. The number of fluorophores per spot was estimated based on the number of photobleaching steps. The density of spots within cells was low enough (~0.1 - 0.25 spots/μm^2) to be confident that single particles were discerned. We also note that the number of miRNAs we observed in the focal plane of a microinjected cell (~500 on average per fixed cell, considering both the number of distinct particles and their individual photobleaching steps; **Supplementary Table 1** and **Fig 4D**) correlates well with the volume fraction of the cell in focus multiplied with the total number of microinjected miRNAs (~18,000), suggesting that we can account for a significant fraction of the microinjected miRNAs.

For mRNA-miRNA colocalization experiments, HeLa cells were co-microinjected with the MS2/MCP plasmids and the appropriate Cy5 labeled miRNA, incubated for 24 h under

normal growth conditions and formaldehyde fixed just prior to imaging. An object based approach [12] was used to quantitatively assess co-localization based on sub-pixel localization of the centers of mass (COMs) of isolated objects from the GFP (green circles) and Cy5 (red circles) channels (**Fig 3C**). Two objects, one from each channel, were considered 'perfectly' co-localized if their COMs were localized in the same pixel (yellow circles) or simply co-localized if the radial distance between the COMs was less than the resolution limit. In the latter case, the COMs of the two co-localized objects occur on adjacent, but separate pixels; these were mapped as cyan and magenta circles for Cy5-COMs and GFP-COMs, respectively, for **Fig. 3C**. We typically observed a density of 0.08 Cy5 particles/μm^2, 0.28 GFP particles/μm^2 and 0.13 Cy5 particles/μm^2, 0.2 GFP particles/μm^2 in the specific (in the presence of target mRNA) and non-specific (with a negative control miRNA) samples, respectively. The density of green particles arising from background fluorescence was 0.08 GFP particles/μm^2 in samples that were injected with mutant let-7-a1-Cy5 (0.07 particles/μm^2) and MCP plasmid without the MS2-mRNA expression plasmid. We chose wild-type let-7-a1 as a non-specific control miRNA for two reasons: (i) This miRNA is incapable of repressing a reporter target with mutant let-7-a1 seed sequences (**Fig 1A**) and (ii) we expect maximal non-specific co-localization of this miRNA with our reporter mRNA in common cellular RNA foci, such as PBs, since let-7-a1 has many endogenous targets that it would localize to PBs, where the mutant mRNA may also reside due to its regulation by endogenous factors. Fluorophore labeled wild-type let-7-a1 thus serves as a robust negative control miRNA, setting an upper limit for sequence independent co-localization.

Repression assays. For transfection repression assays 24 h prior to transfection, 100 μL of 15,000 HeLa cells were seeded per well of a 96 well plate. Cells were transfected with 60 ng of

the indicated plasmid, 10 nM of the indicated dsRNA, 0.4 μL of Lipofectamine 2000 (Invitrogen) and 50 μL of OptiMEM (GIBCO). 6 h after transfection the growth medium was replaced with fresh medium. 24 h after transfection, medium was replaced with phenol red-free DMEM. Dual luciferase assays were performed using the Dual-Glo luciferase assay reagents (Promega) as per the manufacturer's protocol and luminescence was detected using a Genios Pro (Tecan) plate reader. For microinjection repression assays, 0.1 μg/ul of both pEF6-mCherry-mH3UM and pEGFP-C1 plasmids were microinjected with 1.5 μM WT or MUT let-7 miRNA and 0.025% Alexa647 dextran (Invitrogen) in PBS. Following microinjection, cells were maintained under normal growth conditions for 24 h prior to imaging. Fluorescence signal were quantified using ImageJ software (NIH). The background subtracted mCherry signal was normalized with that of GFP for individual cells, which was then averaged over all cells. Using our filter sets (refer to **Microscopy**) we observed a small amount of mCherry bleed-through signal, ~14%, while imaging GFP. This bleed through was corrected for in our calculations. Repression was measured by normalizing the average relative intensity of mutant let-7-a1 injections with respect to that of wild-type let-7-a1 injections.

Estimating the cellular abundance of mRNA targets for let-7 and cxcr4. We first used targetscan 5.2© to identify potential mRNA targets of the let-7 and cxcr4 miRNAs. These targets were then compared to data from a HeLa cell mRNA expression profiling array [13, 14] (dataset accessible at NCBI GEO database [13, 15], accession GSM650992) using a custom written MATLAB code to identify endogenously expressed targets of both miRNAs. We found that ~10% of all predicted targets in either datasets were not expressed in HeLa cells. Comparing

mRNA abundances of all potential targets for both miRNAs, we deduced that let-7 is predicted to have ~10-fold more expressed target molecules than cxcr4.

Calculation of miRNA copy number in HeLa cells. We calculated the number of let-7 miRNA molecules per cell based on miRNA expression profiling data [16] and previously reported abundance of let-7a [17] and miR-21 [18] in HeLa cells. Fluorescence [17] and qRT-PCR [18] assays have estimated the copy number of let-7a and miR-21 to be ~4,000 copies and ~20,000 copies per cell, respectively. Deep sequencing data [16] (http://www.mirz.unibas.ch/cloningprofiles/) suggest that let-7a, which comprises ~16.5% of the total let-7 population, and miR-21 represent ~1.6% and ~13.2%, respectively, of the total miRNA pool in HeLa cells (~150,000 copies). Taking both of these data sets into consideration, we estimate the total let-7 population to be between 15,000 and 24,000 molecules per HeLa cell.

SUPPLEMENTARY REFERENCES

1. Mayr C, Hemann MT, Bartel DP (2007) Disrupting the pairing between let-7 and Hmga2 enhances oncogenic transformation. *Science* **315:** 1576-1579

2. Fusco D, Accornero N, Lavoie B, Shenoy SM, Blanchard JM, Singer RH, Bertrand E (2003) Single mRNA molecules demonstrate probabilistic movement in living mammalian cells. *Curr Biol* **13:** 161-167

3. Wang B, Love TM, Call ME, Doench JG, Novina CD (2006) Recapitulation of short RNA-directed translational gene silencing in vitro. *Molecular cell* **22:** 553-560

4. Walter NG (2003) Probing RNA structural dynamics and function by fluorescence resonance energy transfer (FRET). *Curr Protoc Nucleic Acid Chem* **Chapter 11:** Unit 11 10

5. Walter NG, Burke JM (2000) Fluorescence assays to study structure, dynamics, and function of RNA and RNA-ligand complexes. *Methods Enzymol* **317:** 409-440

6. Tokunaga M, Imamoto N, Sakata-Sogawa K (2008) Highly inclined thin illumination enables clear single-molecule imaging in cells. *Nat Methods* **5:** 159-161

7. Pinaud F, Michalet X, Iyer G, Margeat E, Moore HP, Weiss S (2009) Dynamic partitioning of a glycosyl-phosphatidylinositol-anchored protein in glycosphingolipid-rich microdomains imaged by single-quantum dot tracking. *Traffic* **10:** 691-712

8. Saxton MJ, Jacobson K (1997) Single-particle tracking: applications to membrane dynamics. *Annu Rev Biophys Biomol Struct* **26:** 373-399

9. Kusumi A, Sako Y, Yamamoto M (1993) Confined lateral diffusion of membrane receptors as studied by single particle tracking (nanovid microscopy). Effects of calcium-induced differentiation in cultured epithelial cells. *Biophys J* **65:** 2021-2040

10. Ding H, Wong PT, Lee EL, Gafni A, Steel DG (2009) Determination of the oligomer size of amyloidogenic protein beta-amyloid(1-40) by single-molecule spectroscopy. *Biophys J* **97:** 912-921

11. Chung SH, Kennedy RA (1991) Forward-backward non-linear filtering technique for extracting small biological signals from noise. *J Neurosci Methods* **40:** 71-86

12. Bolte S, Cordelieres FP (2006) A guided tour into subcellular colocalization analysis in light microscopy. *Journal of microscopy* **224:** 213-232

13. Karnani N, Taylor CM, Malhotra A, Dutta A (2010) Genomic study of replication initiation in human chromosomes reveals the influence of transcription regulation and chromatin structure on origin selection. *Molecular biology of the cell* **21:** 393-404

14. Karnani N, Taylor CM, Malhotra A, Dutta A (2010) Genomic study of replication initiation in human chromosomes reveals the influence of transcription regulation and chromatin structure on origin selection. *Mol Biol Cell* **21:** 393-404

15. Barrett T *et al* (2011) NCBI GEO: archive for functional genomics data sets--10 years on. *Nucleic acids research* **39:** D1005-1010

16. Landgraf P *et al* (2007) A mammalian microRNA expression atlas based on small RNA library sequencing. *Cell* **129:** 1401-1414

17. Allawi HT, Dahlberg JE, Olson S, Lund E, Olson M, Ma WP, Takova T, Neri BP, Lyamichev VI (2004) Quantitation of microRNAs using a modified Invader assay. *RNA* **10:** 1153-1161

18. Neilson JR, Zheng GX, Burge CB, Sharp PA (2007) Dynamic regulation of miRNA expression in ordered stages of cellular development. *Genes Dev* **21:** 578-589